Available online at www.sciencedirect.com
SCIENCE DIRECT®
Journal of Sound and Vibration 277 (2004) 895–918
JOURNAL OF SOUND AND VIBRATION
www.elsevier.com/locate/jsvi

Stability of a segmented supercritical driveline with non-constant velocity couplings subjected to misalignment and torque

H.A. DeSmidt[a], K.W. Wang[b,*], E.C. Smith[c]

[a] *The Pennsylvania State University, 7 Hammond Building, University Park, PA 16802, USA*
[b] *The Pennsylvania State University, 157 Hammond Building, University Park, PA 16802, USA*
[c] *The Pennsylvania State University, 233 Hammond Building, University Park, PA 16802, USA*

Received 23 December 2002; accepted 15 September 2003

Abstract

With the trend toward high-speed, lightweight, supercritical drivelines, it is increasingly important to understand all instability phenomena associated with realistic driveline configurations. Furthermore, it is important to understand the interaction between different instability mechanisms. One well-known phenomenon that occurs with supercritical shafts is whirl instability due to internal (rotating-frame) shaft damping. Whirl instability occurs at shaft speeds above the first critical speed and is related to the internal/external-damping ratio. Another less explored instability phenomena is parametric instability caused by non-constant velocity flexible couplings, e.g., U-joint couplings or disk couplings, combined with driveline misalignment and load-torque. Previous research examined stability of various single U-joint/shaft systems without shaft internal damping. However, it is difficult to fully understand the stability of more realistic multi-U-joint/flexible shaft drivelines based on the single U-joint studies due to the more complicated shaft speed kinematics and misalignment configurations of multi-U-joint systems. In this paper, the non-dimensional, linear, periodically time-varying equations-of-motion for a segmented triple-U-joint driveline with shaft internal damping are derived. Torsional and lateral shaft flexibly and their effects on the shaft speed kinematics are included in the model. Numerical Floquet theory is used to explore the effects of internal/external damping ratio, misalignment, load-inertia and load-torque on the stability of the driveline operating at both sub and supercritical speeds. It is discovered that misalignment and load-torque have both stabilizing and destabilizing effects. On one-hand, misalignment and load-torque tend to stabilize internal damping-induced whirl, however, they cause instability at speeds near bending–bending and bending–torsion sum-type combination frequencies. Finally, it is shown that external damping is not always effective for stabilizing the misalignment and torque induced parametric instabilities.

*Corresponding author. Tel.: +1-814-865-2183; fax: +1-814-863-7222.
E-mail address: kwwang@psu.edu (K.W. Wang).

0022-460X/$ - see front matter © 2003 Elsevier Ltd. All rights reserved.
doi:10.1016/j.jsv.2003.09.033

1. Introduction

It is well known that internal shaft (rotating-frame) damping causes whirl instability for shafts operating above their first bending natural frequency. Thus, all drivelines which operate in the supercritical regime require auxiliary fixed-frame lateral damping to prevent instability. Zorzi and Nelson [1], studied the effects of internal damping and gyroscopic effects on the stability of a flexible shaft. Here they derived an expression for the dissipation functions for both shaft viscous and shaft hysteretic damping in fixed-frame co-ordinates. They concluded, that without auxiliary fixed-frame damping, viscous internal damping tended to destabilize the shaft when the rotational speed exceeded the first bending natural frequency. Chen and Ku [2], furthered the stability investigation of supercritical shafts by studying the whirl-speeds using a finite element approach. Here, transverse shear, gyroscopic effects, internal damping, and different boundary conditions were included in the analysis.

Another less recognized source driveline instability is caused by the flexible couplings, which connect the shaft segments. Universal Joints (U-joints) and disk couplings, which have similar kinematics, are widely used in power transmission applications since they are relatively inexpensive and easy to maintain. Additionally, U-joints can accommodate relatively large angular misalignments and have high torque and axial load capacity. Despite these advantages, their non-constant velocity kinematics can lead to undesirable vibration and even instability under certain operating conditions.

Several researchers have investigated the stability of rotor–shaft systems involving a single U-joint coupling. Iwatsubo and Saigo [3] studied the effect of a static follower load-torque on the lateral stability of a nominally aligned rigid rotor–disk mounted on a compliant bearing and driven through a U-joint. They derived expressions for parametric and self-exciting transverse moments created by torque transmitted through the U-joint. It was determined that static load-torque induced parametric instabilities for shaft speeds near the sum-type combinations of the transverse natural frequencies. Mazzei et al. [4] considered the effect of lateral shaft flexibility on the stability of a misaligned shaft driven by a single U-joint subjected to a static follower load-torque. Torsional flexibility was not considered since the shaft was not carrying a rotor–disk or torsional inertia-load. They found that static load-torque caused parametric instability for rotational speeds near sum-type combinations of the shaft bending natural frequencies.

Asokanthan and Hwang [5] and Asokanthan and Wang [6] studied the stability of two torsionally flexible, misaligned shafts coupled by a U-joint. In their analyses the shafts were driving an inertia-load and the lateral shaft orientations were fixed, hence only torsional dynamics were considered. Refs. [5,6] concluded that shaft speed variation due to angular misalignment caused parametric instabilities near principle and sum-type combinations of the torsional natural frequencies. Ref. [5] also concluded that the addition of viscous torsional damping had a stabilizing effect for principle instability zones, but destabilized the sum-type combination instability zones.

DeSmidt et al. [7] considered load-torque, load-inertia and misalignment angle on the stability of a shaft–disk assembly supported on a compliant bearing/damper and driven with a single U-joint. In this analysis, both torsional and lateral flexibility were considered and it was discovered that load-inertia and misalignment together caused periodic inertia coupling of the torsion and lateral modes. This interaction caused torsion–lateral parametric instability for shaft speeds near the torsion–lateral sum combinations. Additionally, it was shown that misalignment

had a stabilizing effect on the load-torque induced flutter instability near the torsional–lateral difference combination frequencies. Finally, Ref. [7] showed that the torsion–lateral instabilities could be stabilized with sufficient lateral viscous damping.

Kato and Ota [8], studied U-joint frictional effects of a misaligned shaft driven by a single U-joint. They concluded that internal friction in the U-joint generates harmonic lateral moments which occur at even multiples of the shaft operating speed, i.e., $2\Omega, 4\Omega, \ldots$, etc. Additionally, they demonstrated that these lateral moments are suppressed if the friction coefficients of the driven and driving yokes are equal.

Several researchers [9–11] investigated the steady-state response of misaligned shaft/U-joint systems. Specifically, Refs. [10,11] studied a laterally flexible, torsionally rigid, shaft between two U-joints using the harmonic balance method. Rosenberg and Ohio [10] considered a double U-joint/shaft–disk system with both joint misalignment angles in the same plane. Here it was discovered that the combination of misalignment and disk imbalance resulted in shaft vibration at odd integer multiple harmonics of the shaft operating speed, i.e., Ω, $3\Omega, \ldots$, etc. Sheu et al. [11], studied the response under a more general misalignment configuration with joint misalignment angles in two orthogonal planes along with shaft imbalance and U-joint friction. Here it was shown that when the U-joints were phased by 90° and the input and output-shafts had the same misalignment, the so-called parallel offset condition, there was no speed variation between input and output-shafts. However, this ideal kinematic condition was distorted by lateral bending vibration of the intermediate shaft, which resulted in harmonic lateral moments at even multiples of the operating speed. Additionally, it was shown that differences between U-joint friction coefficients caused axial torque fluctuations.

2. Problem statement and research objective

As illustrated in Section 1, many researchers have studied the stability of shafts operating at supercritical speeds, where it has been shown that internal (rotating-frame) damping tends to cause whirl instability dependinthe amount of external (fixed-frame) damping present. However, the effect of non-constant velocity couplings has not been included in these analyses. Some researchers explored the stability of single U-joint/shaft–disk systems, where its been shown that misalignment and load-torque generate periodic parametric terms that cause instability near certain shaft speeds. While the results were interesting, the single U-joint system does not really resemble a typical driveline. Furthermore, previous analyses of double U-joint/shaft systems only considered the periodic moment forcing terms, but neglected the potentially destabilizing periodic parametric terms. Hence, the stability behavior of a segmented driveline involving multiple non-constant velocity couplings has not been studied. Since most drivelines consist of two or more flexible couplings, depending on the number of segments, it is important to understand the effect of misalignment and load-torque on the stability of such multi-coupling/shaft systems. Furthermore, with the trend toward supercritical drivelines, the interaction between different instability regions due to misalignment, load-torque and the rotating-frame damping-induced whirl instability must be assessed. The objective of this research is to address these issues and investigate the stability of a multi-segment supercritical driveline with non-constant velocity couplings subjected to misalignment and torque.

3. System description and equations of motion

Equations of motion are derived for the segmented driveline system shown in Fig. 1. The system consists of a fixed input-shaft, a fixed output-shaft and two flexible intermediate shafts with length L. The shafts are connected by U-joint couplings A, B and C, that are nominally phased about the rotation axis by 90°, as is typically the case. Specifically, the U-joint phase angles are $\psi_A = 0$, $\psi_B = \pi/2$ and $\psi_C = 0$. The intermediate shafts are flexible in bending and torsion and are supported on a rigid bearing. Also, the U-joints are assumed to be rigid in the transverse directions thus giving the intermediate shaft segments pinned–pinned transverse boundary conditions. Two mid-span dampers, with damping coefficient C_d, provide auxiliary lateral viscous damping in the fixed-frame to counteract the destabilizing effects of the shaft internal damping.

Here, $\{\mathbf{m}\} = [\mathbf{m}_1, \mathbf{m}_2, \mathbf{m}_3]$ is a fixed co-ordinate frame aligned with the intermediate shafts with $\mathbf{m}_2$ into the page. The transverse displacements measured from the $\{\mathbf{m}\}$ frame are defined as

$$v(x,t) = \begin{cases} v_1(x,t), & 0 \leqslant x \leqslant L, \\ v_2(x-L,t), & L \leqslant x \leqslant 2L, \end{cases}$$
$$w(x,t) = \begin{cases} w_1(x,t), & 0 \leqslant x \leqslant L, \\ w_2(x-L,t), & L \leqslant x \leqslant 2L, \end{cases} \tag{1}$$

where $v(x,t)$ and $w(x,t)$ measure deflection in the $\mathbf{m}_2$ and $\mathbf{m}_3$ directions. The total shaft rotational angle, $\phi(x,t)$, and elastic windup angle, $\hat{\phi}(x,t)$, are defined as

$$\phi(x,t) = \begin{cases} \phi_1(x,t) = \bar{\phi}_1(t) + \hat{\phi}_1(x,t), & 0 \leqslant x \leqslant L, \\ \phi_2(x-L,t) = \bar{\phi}_2(t) + \hat{\phi}_2(x-L,t), & L \leqslant x \leqslant 2L, \end{cases}$$
$$\phi(x,t) = \begin{cases} \hat{\phi}_1(x,t), & 0 \leqslant x \leqslant L, \\ \hat{\phi}_2(x-L,t), & L \leqslant x \leqslant 2L, \end{cases} \tag{2}$$

where $\bar{\phi}_i(x,t)$ are rigid-body rotations and $\hat{\phi}_i(x,t)$ are elastic twist deformations of the intermediate shafts. It is assumed that the input-shaft is driven at a constant speed, Ω_0, and the

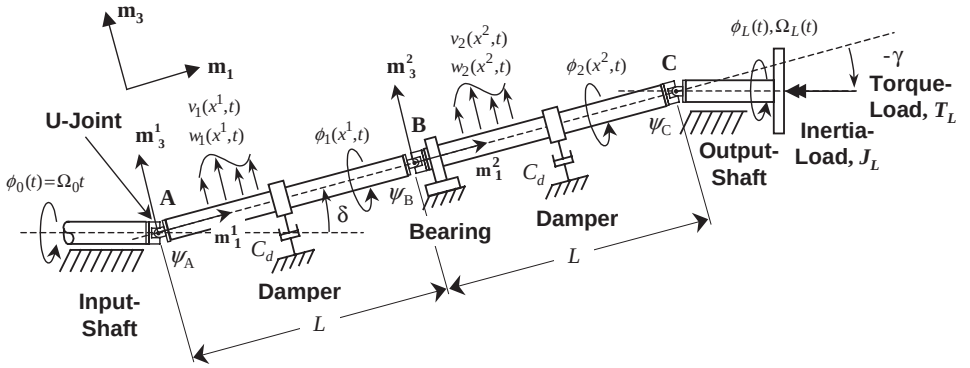

Fig. 1. Segmented driveline with inertia and torque loads, subjected to input and output-shaft misalignments δ and γ.

output-shaft drives both a torsional inertia-load, J_L, and a resistive torque-load, T_L, with rotation angle ϕ_L, and rotation speed Ω_L. Finally, it is assumed that the driveline is subjected to static angular misalignments, δ and γ, in the $\mathbf{m}_1$–$\mathbf{m}_3$ plane at the input- and output-shafts, respectively.

Since U-joints have non-constant velocity kinematics, the rotation speed of the shaft segments deviate from each other as a function of the angular misalignment between the segments. Fig. 2 shows the **P**th U-joint, with phase angle ψ_P, connecting the misaligned flexible shaft segments $i-1$ and i of lengths L_{i-1} and L_i.

The total effective misalignment is the sum of the nominal static misalignments, $\theta_{v,P}$ and $\theta_{w,P}$, plus the net dynamic misalignments at the **P**th coupling due to bending. The dynamic misalignments at the **P**th coupling are defined in terms of the elastic slopes as $v'_p = v'_{i,P} - v'_{i-1,P}$ and $w'_P = w'_{i,P} - w'_{i-1,P}$, where

$$\begin{aligned} v'_{i-1,P} &\equiv v'_{i-1}(x,t)\big|_{x=L_{i-1}}, \quad v'_{i,P} \equiv v'_i(x,t)\big|_{x=0}, \\ w'_{i-1,P} &\equiv w'_{i-1}(x,t)\big|_{x=L_{i-1}}, \quad w'_{i,P} \equiv w'_i(x,t)\big|_{x=0}. \end{aligned} \tag{3}$$

Here, the "′ " indicates differentiation with respect to the axial co-ordinate, x. The total rotation angle of the $i-1$th shaft at the **P**th U-joint due to rigid-body rotation and elastic windup is $\phi_{i-1,P}(t)$.

$$\phi_{i-1,P}(t) = \bar{\phi}_{i-1}(t) + \hat{\phi}_{i-1}(x,t)\big|_{x=L_{i-1}}. \tag{4}$$

Using the kinematic expression derived in Ref. [7] for the U-joint driven-yoke spin angle, the rotation co-ordinate, $\phi_i(x,t)$, of the ith shaft can be expressed as

$$\phi_i(x,t) = \bar{\phi}_i(t) + \hat{\phi}_i(x,t), \quad 0 < x < L_i \tag{5a}$$

with

$$\begin{aligned} \bar{\phi}_i(t) = \bar{\phi}_{i-1}(t) &+ \frac{\sin(2[\phi_{i-1,P} + \psi_P])}{4}[(v'_P + \theta_{v,P})^2 - (w'_P + \theta_{w,P})^2] \\ &- \frac{\cos(2[\phi_{i-1,P} + \psi_P])}{2}(v'_P + \theta_{v,P})(w'_P + \theta_{w,P}) \\ &+ \tfrac{1}{2}(\theta_{v,P} + v'_{i,P})(\theta_{w,P} - w'_{i-1,P}) - \tfrac{1}{2}(\theta_{w,P} + w'_{i,P})(\theta_{v,P} - v'_{i-1,P}). \end{aligned} \tag{5b}$$

By successively applying Eq. (5) starting with the input-shaft, $i-1=0$, with given input rotation angle, $\phi_0 = \bar{\phi}_0 = \Omega_0 t$, at U-joint A, and proceeding through U-joints B and C to the output-shaft, expressions for the intermediate and output-shaft rotation angles, $\phi(x,t)$ and $\phi_L(t)$, are obtained.

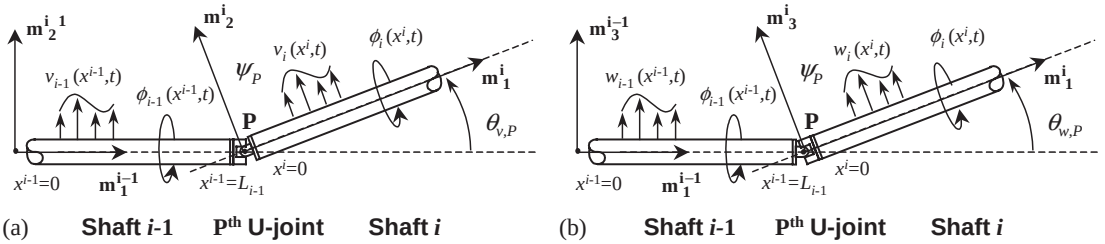

Fig. 2. **P**th U-joint connecting nominally misaligned shafts $i-1$ and i. (a) $\mathbf{m}_1 - \mathbf{m}_2$ plane and (b) $\mathbf{m}_1 - \mathbf{m}_3$ plane.

Eq. (6) shows the output-shaft rotation angle:

$$\begin{aligned}\phi_L(t) = {} & \hat{\phi}_{2,C} + \phi_0 + \tfrac{1}{2}\Big(\delta v'_{1,A} + v'_{1,B}w'_{2,B} - v'_{2,B}w'_{1,B} + \gamma v'_{2,C}\Big) + \tfrac{\delta^2}{8}\Big(v'_{2,C}(\gamma - w'_{2,C}) + v'_B w'_B\Big) \\ & + \tfrac{1}{4}\sin(2\phi_0)\Big[v'^2_{1,A} - (\delta + w'_{1,A})^2 - 4\hat{\phi}_{1,B}v'_B w'_B - (1 - 2\hat{\phi}^2_{1,B})(v'^2_B - w'^2_B)\Big] \\ & - \tfrac{1}{4}\sin(2\phi_0)\Big[4\hat{\phi}_{2,C}v'_{2,C}(\gamma - w'_{2,C}) - (1 - 2\hat{\phi}^2_{2,C})(v'^2_{2,C} - (\gamma - w'_{2,C})^2)\Big] \\ & - \tfrac{1}{2}\cos(2\phi_0)\Big[(\delta + w'_{1,A})v'_{1,A} - (1 - 2\hat{\phi}^2_{1,B})v'_B w'_B + \hat{\phi}_{1,B}(v'^2_B - w'^2_B)\Big] \\ & + \tfrac{1}{2}\cos(2\phi_0)\Big[(1 - 2\hat{\phi}^2_{2,C})v'_{2,C}(\gamma - w'_{2,C}) + \hat{\phi}_{2,C}(v'^2_{2,C} - (\gamma - w'_{2,C})^2)\Big]\end{aligned} \tag{6a}$$

with elastic windup angles at U-joints B and C defined as

$$\hat{\phi}_{1,B}(t) = \phi_{sB} + \hat{\phi}_1(x,t)\big|_{x=L} \quad \text{and} \quad \hat{\phi}_{2,C}(t) = \phi_{sC} + \hat{\phi}_2(x,t)\big|_{x=L}, \tag{6b}$$

where ϕ_{sB} and ϕ_{sC} are static portions of the elastic windup due to the torque-load, T_L. In the above expressions small misalignments are assumed, i.e., δ and $\gamma \leqslant 10^\circ$. Finally, differentiating the shaft rotation angles with respect to time yields the intermediate and output-shaft rotation speeds, $\Omega(x,t) = \dot{\phi}(x,t)$and $\Omega_L(t) = \dot{\phi}_L(t)$, where the "˙" indicates time differentiation.

The kinetic energy of the driveline system is

$$T = \int_0^{2L}\left[\frac{m}{2}(\dot{v}^2 + \dot{w}^2) + \frac{I_m}{2}(\dot{v}'^2 + \dot{w}'^2) + \frac{J_m}{2}\left(\Omega^2 + \Omega[w'\dot{v}' - v'\dot{w}']\right)\right]\mathrm{d}x + \frac{J_L}{2}\Omega_L^2, \tag{7}$$

where m is the shaft mass per unit length and I_m and J_m are the shaft cross-sectional transverse and polar mass moments of inertia. Since, it is assumed that $J_m L \ll J_L$, the effect of the intermediate shaft speed variation on the equations-of-motion is negligible compared to the effect of the output-shaft speed variation. Hence the full expressions for $\phi_L(t)$ and $\Omega_L(t)$ are used in the derivation but $\phi(x,t)$ and $\Omega(x,t)$ are approximated as

$$\phi(x,t) \approx \Omega_0 t + \hat{\phi}(x,t) \quad \text{and} \quad \Omega(x,t) \approx \Omega_0 + \dot{\hat{\phi}}(x,t). \tag{8}$$

The driveline strain energy is expressed as

$$V = \int_0^{2L}\left[\frac{EI}{2}(v''^2 + w''^2) + \frac{GJ}{2}\hat{\phi}'^2\right]\mathrm{d}x. \tag{9}$$

here E and G are the shaft material elastic and shear moduli and I and J are the cross-sectional transverse and polar area moments of inertia. To account for shaft structural damping in the rotating-frame and auxiliary damping in the fixed-frame, a Rayleigh dissipation function, D, is constructed similar to [1]

$$\begin{aligned}D = {} & \xi_v \int_0^{2L}\left[\frac{EI}{2}(\dot{v}''^2 + \dot{w}''^2 + 2\Omega_0[\dot{v}''w'' - \dot{w}''v''] + \Omega_0^2[v''^2 + w''^2]) + \frac{GJ}{2}\dot{\hat{\phi}}'^2\right]\mathrm{d}x \\ & + \frac{C_d}{2}(\dot{v}^2 + \dot{w}^2)\bigg|_{x=L/2} + \frac{C_d}{2}(\dot{v}^2 + \dot{w}^2)\bigg|_{x=L+L/2}.\end{aligned} \tag{10}$$

here ξ_v is the shaft material loss-factor and C_d is the fixed-frame damper damping coefficient.

To obtain equations-of-motion, the transverse deflections, $v(x,t)$ and $w(x,t)$, and elastic twisting, $\hat{\phi}(x,t)$, are written in terms of the modal expansion

$$v(x,t) = \Phi_v(x)\eta(t), \quad w(x,t) = \Phi_w(x)\eta(t), \quad \hat{\phi}(x,t) = \Phi_\phi(x)\eta(t), \tag{11}$$

where $\eta(t)$ is the $n \times 1$ column vector of modal co-ordinates and $\Phi_v(x)$, $\Phi_w(x)$ and $\Phi_\phi(x)$ are the corresponding row vectors of assumed mode shapes:

$$\Phi_v(x) = \begin{cases} \Phi_{v1}(x) = [L\ \sin\frac{\pi x}{L} \quad 0 \quad 0 \quad 0 \quad L\sin\frac{2\pi x}{L} \quad 0 \quad 0 \quad 0 \quad 0], & 0 \leqslant x \leqslant L, \\ \Phi_{v2}(x) = [0 \quad 0 \quad L\sin\frac{\pi(x-L)}{L} \quad 0 \quad 0 \quad 0 \quad L\sin\frac{2\pi(x-L)}{L} \quad 0 \quad 0], & L \leqslant x \leqslant 2L, \end{cases}$$

$$\Phi_w(x) = \begin{cases} \Phi_{w1}(x) = [0 \quad L\sin\frac{\pi x}{L} \quad 0 \quad 0 \quad 0 \quad L\sin\frac{2\pi x}{L} \quad 0 \quad 0 \quad 0], & 0 \leqslant x \leqslant L, \\ \Phi_{w2}(x) = [0 \quad 0 \quad 0 \quad L\sin\frac{\pi(x-L)}{L} \quad 0 \quad 0 \quad 0 \quad L\sin\frac{2\pi(x-L)}{L} \quad 0], & L \leqslant x \leqslant 2L, \end{cases}$$

$$\Phi_\phi(x) = \left[0 \quad 0 \quad 0 \quad 0 \quad 0 \quad 0 \quad 0 \quad 0 \quad \frac{x}{2L}\right], \quad 0 \leqslant x \leqslant 2L. \tag{12}$$

here, $\Phi_v(x)$ and $\Phi_w(x)$, contain the first two pinned–pinned bending mode shapes for both intermediate shafts and $\Phi_\phi(x)$, is composed of the first fixed–free twisting mode shape.

After substitution of the modal expansions given in Eqs. (11) and (12), the functional representation of the output-shaft speed and rotation angle becomes

$$\phi_L = \phi_L(t, \Omega_0, \delta, \gamma, \eta) \quad \text{and} \quad \Omega_L = \Omega_L(t, \Omega_0, \delta, \gamma, \eta, \dot{\eta}). \tag{13}$$

The virtual work, δW_{T_L}, and corresponding generalized force vector, Q_{T_L}, due to the output-shaft resistive torque load, T_L, are written as

$$\delta W_{T_L} = -T_L \delta\phi_L \equiv Q_{T_L}^{\mathrm{T}} \delta\eta \quad \text{with} \quad \delta\phi_L = \left[\frac{\partial \phi_L}{\partial \eta}\right]^{\mathrm{T}} \delta\eta, \quad \text{thus} \quad Q_{T_L} = -T_L \frac{\partial \phi_L}{\partial \eta}. \tag{14}$$

After substituting the modal expansions into the energy and dissipation expressions in Eqs. (7), (9) and (10), the equation-of-motion, is obtained via Lagrange's equation:

$$\begin{aligned} &\frac{\mathrm{d}}{\mathrm{d}t}\left[\frac{\partial T}{\partial \dot{\eta}}\right] - \frac{\partial T}{\partial \eta} + \frac{\partial V}{\partial \eta} + \frac{\partial D}{\partial \dot{\eta}} - Q_{T_L} \\ &= \underbrace{\mathbf{M}\ddot{\eta} + [\mathbf{G} + \mathbf{C}_{sd} + \mathbf{C}_{aux}]\dot{\eta} + [\mathbf{K} + \mathbf{K}_{rd}]\eta}_{\text{Nominal system}} + \underbrace{J_L \dot{\Omega}_L \frac{\partial \Omega_L}{\partial \dot{\eta}} + J_L \Omega_L \left(\frac{\mathrm{d}}{\mathrm{d}t}\left[\frac{\partial \Omega_L}{\partial \dot{\eta}}\right] - \frac{\partial \Omega_L}{\partial \eta}\right) + T_L \frac{\partial \phi_L}{\partial \eta}}_{\text{Misalignment \& torque terms}} = 0, \end{aligned} \tag{15}$$

where nominal system matrices are

$$\mathbf{M} = \int_0^{2L} \left[m(\Phi_v^{\mathrm{T}}\Phi_v + \Phi_w^{\mathrm{T}}\Phi_w) + I_m(\Phi_v'^{\mathrm{T}}\Phi_v' + \Phi_w'^{\mathrm{T}}\Phi_w') + J_m\left(\Phi_\phi^{\mathrm{T}}\Phi_\phi\right)\right] \mathrm{d}x,$$

$$\mathbf{G} = J_m\Omega_0 \int_0^{2L} [\Phi_v'^{\mathrm{T}}\Phi_w' - \Phi_w'^{\mathrm{T}}\Phi_v'] \,\mathrm{d}x$$

$$\mathbf{C}_{sd} = \xi_v \int_0^{2L} \left[EI(\Phi_v''^{\mathrm{T}}\Phi_v'' + \Phi_w''^{\mathrm{T}}\Phi_w'') + GJ(\Phi_\phi'^{\mathrm{T}}\Phi_\phi')\right] \mathrm{d}x,$$

$$\mathbf{C}_{aux} = c_d\left[(\Phi_v^{\mathrm{T}}\Phi_v + \Phi_w^{\mathrm{T}}\Phi_w)\big|_{x=L/2} + (\Phi_v^{\mathrm{T}}\Phi_v + \Phi_w^{\mathrm{T}}\Phi_w)\big|_{x=3L/2}\right],$$

$$\mathbf{K} = \int_0^{2L} \left[EI(\Phi_v''^{\mathrm{T}}\Phi_v'' + \Phi_w''^{\mathrm{T}}\Phi_w'') + GJ(\Phi_\phi'^{\mathrm{T}}\Phi_\phi')\right] \mathrm{d}x,$$

$$\mathbf{K}_{rd} = \xi_v EI\Omega_0 \int_0^{2L} [\Phi_v''^{\mathrm{T}}\Phi_w'' - \Phi_w''^{\mathrm{T}}\Phi_v''] \,\mathrm{d}x, \tag{16}$$

$\mathbf{M}, \mathbf{G}$ and $\mathbf{K}$ are shaft inertia, gyroscopic and elastic stiffness matrices, $\mathbf{C}_{sd}$ and $\mathbf{C}_{aux}$ are the shaft structural and auxiliary damping matrices, and $\mathbf{K}_{rd}$ is the skew-symmetric stiffness matrix due to the rotating-frame damping. The terms due to misalignment, load-inertia and load-torque are obtained by substituting the expressions for ϕ_L and Ω_L into Eq. (15) and taking the necessary partial and time derivatives. After this procedure it becomes apparent that

$$\frac{\mathrm{d}}{\mathrm{d}t}\left[\frac{\partial\Omega_L}{\partial\dot{\eta}}\right] - \frac{\partial\Omega_L}{\partial\eta} = 0. \tag{17}$$

After substituting Eq. (17) into Eq. (15), the resulting terms due to misalignment and load-inertia are reduced to, $J_L\dot{\Omega}_L(\partial\Omega_L/\partial\dot{\eta})$, and terms due to misalignment and load-torque are $T_L(\partial\phi_L/\partial\eta)$. By assuming the dynamic misalignments are an order-of-magnitude smaller than the static misalignments and dropping higher-order terms, the equation-of-motion becomes linearized. In the following Eq. (18a) is the nominal equation-of-motion, which assumes no misalignment and no load-torque. Furthermore, Eq. (18b) gives the full equation-of-motion that contains periodically time-varying parametric and forcing terms due to misalignment, load-inertia, and load-torque

$$\bar{\mathbf{M}}\,\overset{**}{\bar{\eta}} + \left[\bar{\mathbf{G}} + \bar{\mathbf{C}}_{sd} + \bar{\mathbf{C}}_{aux}\right]\overset{*}{\bar{\eta}} + \left[\bar{\mathbf{K}} + \bar{\mathbf{K}}_{rd}\right]\bar{\eta} = \mathbf{0}, \tag{18a}$$

$$\begin{aligned}\bar{\mathbf{M}}\,\overset{**}{\bar{\eta}} + \left[\bar{\mathbf{G}} + \bar{\mathbf{C}}_{sd} + \bar{\mathbf{C}}_{aux}\right]\overset{*}{\bar{\eta}} + \left[\bar{\mathbf{K}} + \bar{\mathbf{K}}_{rd}\right]\bar{\eta} + \left[\bar{\mathbf{M}}_0 + \bar{\mathbf{M}}_{c2}\cos(2f_0\bar{t}) + \bar{\mathbf{M}}_{s2}\sin(2f_0\bar{t})\right]\overset{**}{\bar{\eta}}\\ + \left[\bar{\mathbf{C}}_0 + \bar{\mathbf{C}}_{c2}\cos(2f_0\bar{t}) + \bar{\mathbf{C}}_{s2}\sin(2f_0\bar{t})\right]\overset{*}{\bar{\eta}} + \left[\bar{\mathbf{K}}_0 + \bar{\mathbf{K}}_{c2}\cos(2f_0\bar{t}) + \bar{\mathbf{K}}_{s2}\sin(2f_0\bar{t})\right]\bar{\eta}\\ = \bar{\mathbf{F}}_0 + \bar{\mathbf{F}}_{c2}\cos(2f_0\bar{t}) + \bar{\mathbf{F}}_{s2}\sin(2f_0\bar{t}).\end{aligned} \tag{18b}$$

Here the equations have been non-dimensionalized with respect to the first pinned–pinned bending frequency, Ω_{ND}, and the intermediate shaft segment length L. The "$*$" operator indicates differentiation with respect to non-dimensional (ND) time, $\bar{t}$. The relevant ND parameters for a solid circular cross-section shaft are shown in below, and the ND matrices in Eq. (18) are defined

in Appendix A:

$$\Omega_{ND} = \sqrt{\frac{EI\pi^4}{mL^4}}, \quad \bar{t} = t\Omega_{ND}, \quad \bar{x} = \frac{x}{L}, \quad \bar{v} = \frac{v}{L}, \quad \bar{w} = \frac{w}{L}, \quad \varepsilon = \frac{d}{L}, \tag{19}$$

where the ND shaft displacements are $\bar{v}$, $\bar{w}$ and the ND axial co-ordinate is $\bar{x}$. Also, the shaft slenderness ratio based on diameter, d, is ε:

$$\mu = \frac{J_L}{mL^3}, \quad \tau = \frac{T_L}{mL^3\Omega_{ND}^2}, \quad \tau_{\max} = \frac{2\varepsilon_{shear}}{\varepsilon\pi^4(1+\upsilon)}, \quad k_\phi = \frac{1}{2\pi^4(1+\upsilon)}, \quad \phi_s = -\frac{\tau}{k_\phi}. \tag{20}$$

Also, μ and τ are the ND load-inertia and load-torque parameters and $\tau_{\max}$ is the maximum load-torque parameter based on the material shear-yield strain, ε_{shear}, and the Poisson ratio, υ. The ND torsion stiffness is, k_ϕ, and the static windup angle of the driveline at U-joint C, due to τ, is ϕ_s:

$$f_0 = \frac{\Omega_0}{\Omega_{ND}}, \quad f_1 = \sqrt{\frac{1}{1+\varepsilon^2\pi^2/16}} \approx 1,$$
$$f_2 = 4\sqrt{\frac{1}{1+\varepsilon^2\pi^2/4}} \approx 4, \quad f_\phi = \sqrt{\frac{k_\phi}{\mu+\varepsilon^2/12}} \approx \sqrt{\frac{k_\phi}{\mu}}. \tag{21}$$

The ND input-shaft speed is f_0, the first two ND bending natural frequencies are f_1 and f_2 and the first ND torsion natural frequency is f_ϕ.

$$\bar{\xi}_v = \xi_v\Omega_{ND}, \quad c_d = \frac{C_d}{mL\Omega_{ND}}, \quad r_d = \frac{c_d}{\bar{\xi}_v}. \tag{22}$$

Furthermore, $\bar{\xi}_v$ is the ND shaft material damping loss-factor, c_d is the ND auxiliary damping coefficient and r_d is the ratio of external to internal damping. Finally, the driveline equation-of-motion (18) is valid under the parameter constraints:

$$\varepsilon \ll 1, \quad J_m L \ll J_L \quad \Rightarrow \quad f_\phi \ll \frac{2}{\varepsilon\pi^2}\sqrt{\frac{3}{5(1+\upsilon)}}, \quad \tau < \tau_{\max}. \tag{23}$$

In Eq. (18), the ND nominal system matrices are $\bar{\mathbf{M}}, \bar{\mathbf{G}}, \bar{\mathbf{C}}_{sd}, \bar{\mathbf{C}}_{aux}, \bar{\mathbf{K}}$, and $\bar{\mathbf{K}}_{rd}$ and the remaining matrices are due the non-constant velocity effects combined with misalignment, load-inertia and load-torque. Specifically, the inertia matrices, $\bar{\mathbf{M}}_0, \bar{\mathbf{M}}_{c2}$ and $\bar{\mathbf{M}}_{s2}$, and damping matrices, $\bar{\mathbf{C}}_0, \bar{\mathbf{C}}_{c2}$ and $\bar{\mathbf{C}}_{s2}$, are functions of the misalignment angles, δ and γ, and inertia-load parameter, μ. Moreover, the stiffness matrices, $\bar{\mathbf{K}}_0, \bar{\mathbf{K}}_{c2}$ and $\bar{\mathbf{K}}_{s2}$, and forcing terms, $\bar{\mathbf{F}}_0, \bar{\mathbf{F}}_{c2}$ and $\bar{\mathbf{F}}_{s2}$, are functions of δ, γ, μ along with the load-torque parameter, τ, and the static windup angle ϕ_s.

4. Stability analysis

In the following sub-sections, the stability behavior of Eqs. (18a) and (18b) is analyzed. To establish a baseline for studying the stability of the full system (18b), the effect of shaft internal and external damping on the stability of the nominal system (18a) is first examined. Next, the stability of the full system is explored including the effects of internal and external damping, driveline misalignment, and load-torque.

As a basis for analysis, the parameters of a typical supercritical driveline are used in the equations. The shaft slenderness ratio is $\varepsilon = 0.012$ and the ND material loss-factor is $\bar{\xi}_v = 0.004$, which corresponds a 0.2% first mode damping ratio typical for metal alloy shafts. Furthermore, the shaft material shear yield strain is $\varepsilon_{shear} = 2.7 \times 10^{-3}$, and the Poisson ratio, υ, is 0.3. Finally, the inertia-load parameter is, $\mu = 0.253$, which corresponds to a ND torsional natural frequency of $f_\phi = 0.125$. All the above parameters satisfy the constraints given in Eq. (23). The remaining ND parameters, e.g., misalignment angles, δ and γ, load-torque, τ, external damping coefficient, c_d, and shaft operating speed, f_0, will be varied to explore the stability behavior.

4.1. Nominal system stability

With no misalignment and no load-torque ($\delta = 0, \gamma = 0$ and $\tau = 0$), the driveline dynamics are described by the linear time-invariant nominal system in Eq. (18a). In this case, like in Refs. [1,2], the destabilizing mechanism is the rotating-frame shaft damping, $\bar{\xi}_v$, which gives rise to both the structural damping matrix, $\mathbf{C}_{sd}$, and the destabilizing skew-symmetric stiffness matrix, $\mathbf{K}_{rd}$. Fig. 3 shows the whirl stability behavior in terms of the shaft speed, f_0, and the external to internal damping ratio, r_d.

The nominal system is stable for all sub-critical operation speeds, regardless of damping. For supercritical shaft speeds, $f_0 > f_1$, external damping, c_d, is required for stable operation. In this analysis the external dampers are located at the mid-span of both shaft segments, which is the nodal point of the second bending mode, therefore increasing the external to internal damping ratio increases the first mode whirl-speed but has no effect on the second mode whirl-speed. This represents a practical situation for supercritical drivelines where it may be impossible to provide external damping to all of the higher modes.

The ith mode whirl-speed is defined as the shaft speed at which the real part of the ith mode eigenvalue first becomes positive and the mode becomes unstable. The overall whirl-speed

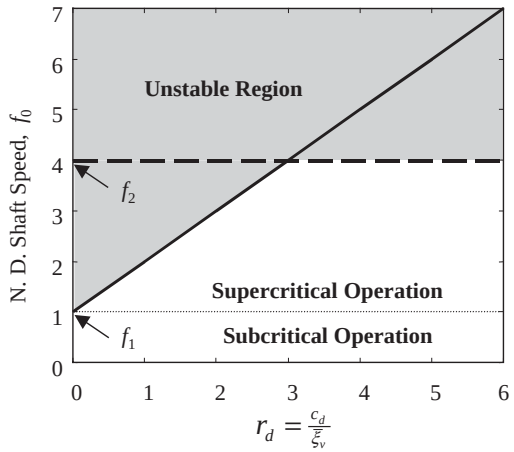

Fig. 3. Nominal system whirl stability: —, first mode critical speed, - - -, second mode critical speed.

is defined as the slowest speed at which whirl instability occurs. Eq. (24) shows the first and second mode whirl-speeds, f_{w_1} and f_{w_2}, and the overall whirl-speed, f_w, for the nominal system:

$$f_{w_1} = \frac{c_d}{2\zeta} + f_1, \quad f_{w_2} = f_2, \quad f_w = \min(f_{w_1}, f_{w_2}). \tag{24}$$

Since, in this case, external damping does not increase the second mode whirl-speed, the largest achievable stable shaft speed range for the nominal system is $0 \leqslant |f_0| < f_2$.

4.2. Full system stability

When misalignment and load-torque are present, the driveline dynamics are described by the linear, periodic time-varying system given by Eq. (18b). In this analysis, the stability is determined numerically via Floquet theory by examining the eigenvalues of the Floquet Transition Matrix (FTM), see Ref. [12]. This technique is numerically intensive but deemed necessary to capture all the instability behavior of the system.

With Eq. (18b) recast in first order form and the forcing terms set to zero, the system is written as

$$\overset{*}{\mathbf{X}} = \mathbf{A}(\bar{t})\mathbf{X} \quad \text{with } \mathbf{X} = [\bar{\eta} \quad \overset{*}{\bar{\eta}}]^{\mathrm{T}} \quad \text{and } \mathbf{A}(\bar{T} + \bar{t}) = \mathbf{A}(\bar{t}), \tag{25}$$

where $\mathbf{A}(\bar{t})$ is the $2n \times 2n$ periodic system matrix and $\mathbf{X}$ is the state vector. $\bar{T}$ is the ND period, which is $\bar{T} = \pi/f_0$. Next, the FTM matrix, denoted by $\Phi(\bar{T})$, is generated, where

$$\Phi(\bar{T}) = [\{\mathbf{x}_1(\bar{T})\}, \{\mathbf{x}_2(\bar{T})\}, \ldots, \{\mathbf{x}_{2n}(\bar{T})\}] \tag{26}$$

and $[\{\mathbf{x}_1(\bar{T})\}, \{\mathbf{x}_2(\bar{T})\}, \ldots, \{\mathbf{x}_{2n}(\bar{T})\}]$ are the $2n$ linearly independent solutions obtained by numerically integrating equation (25) from 0 to $\bar{T}$ with the initial conditions

$$\Phi(0) = \begin{bmatrix} 1 & 0 & \cdots & 0 \\ 0 & 1 & \cdots & 0 \\ \vdots & \vdots & \ddots & 0 \\ 0 & 0 & 0 & 1 \end{bmatrix}_{2n \times 2n}. \tag{27}$$

The FTM matrix, $\Phi(\bar{T})$, maps the state of the system from some initial state, $\mathbf{X}_0$, to the state at time $\bar{t} = k\bar{T}$, such that $\mathbf{X}(k\bar{T}) = \Phi(\bar{T})^k \mathbf{X}_0$, where k is an integer. Thus the eigenvalues, λ_i, of $\Phi(\bar{T})$, which govern the stability of the mapping, also determine the stability of the system.

As discussed in Ref. [13], it is expected that parametric instabilities may occur when the parameter variation frequency, which in this case is $2f_0$, is in the neighborhood of the principal, sum, and difference combination frequencies. Thus the potential shaft speed parametric instability zones are summarized as

$$f_0 = \left| \frac{\omega_{n_i} \pm \omega_{n_j}}{2k} \right| + \rho, \quad \text{for } [i, j, k = 1, 2, 3, \ldots], \tag{28}$$

where ω_{n_i} and ω_{n_j} are system natural frequencies and ρ is a small frequency de-tuning parameter.

Fig. 4 and 5 show how the stability varies with the degree misalignment over the shaft speed range, $0 \leqslant |f_0| < f_2$, for several values of external damping, c_d, and load-torque, τ. Fig. 4 gives the

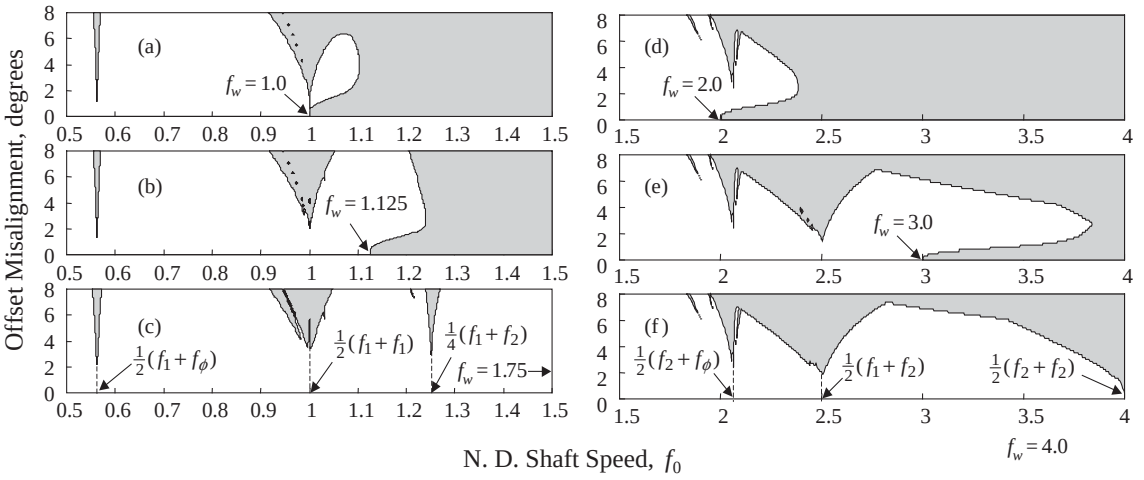

Fig. 4. Misalignment-shaft speed instablity region, $\tau = 0.0$. □, unstable region: (a) $c_d = 0.0$, (b) $c_d = 0.0005$, (c) $c_d = 0.003$, (d) $c_d = 0.004$, (e) $c_d = 0.008$, and (f) $c_d = 0.02$.

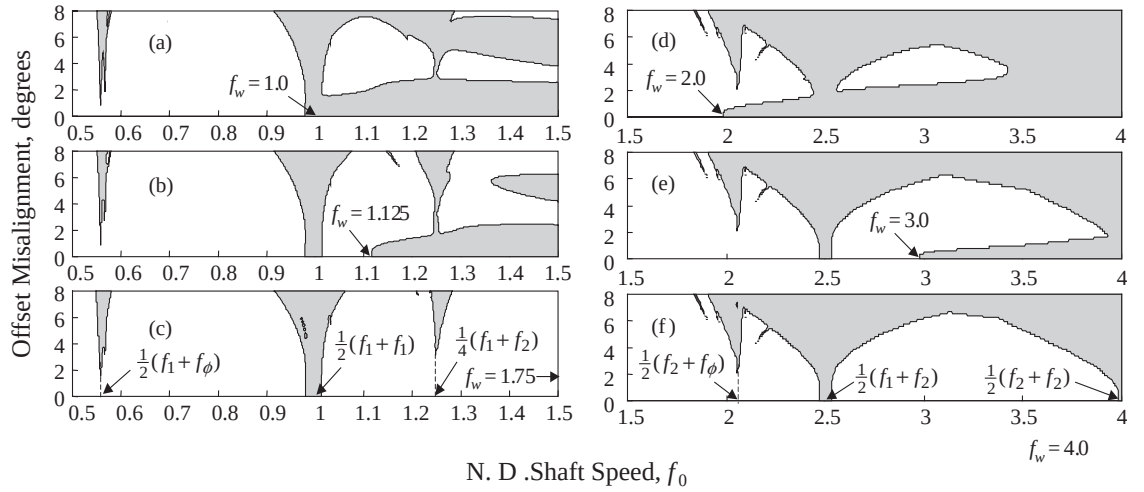

Fig. 5. Misalignment-shaft speed instablity region, $\tau = 0.5\tau_{\max}$. □, unstable region: (a) $c_d = 0.0$, (b) $c_d = 0.0005$, (c) $c_d = 0.003$, (d) $c_d = 0.004$, (e) $c_d = 0.008$, and (f) $c_d = 0.02$.

results for the case with $\tau = 0$ and Fig. 5 gives results for $\tau = 0.5\tau_{\max}$. The misalignment condition is a so-called offset misalignment, with $\delta = -\gamma$, where the input and output-shafts remain parallel but are offset by some distance.

Fig. 4 demonstrates that misalignment has both stabilizing and destabilizing effects. On one hand, for a given nominal whirl-speed, f_w, corresponding to a the external/internal damping ratio, r_d, small amounts of misalignment increase the effective whirl-speed by delaying the onset of instability to speeds above f_w. Thus, misalignment tends to stabilize the whirl instability induced

by internal damping. On the other hand, despite this stabilizing effect, higher values of misalignment cause parametric instability for shaft speeds near the sum-type combinations of the system natural frequencies.

For the case with no external damping, $c_d = 0$, corresponding to $f_w = 1$ (Fig. 4a) it is seen that increasing the misalignment from 0° to about 2° delays the whirl instability from $f_0 = 1$ to around $f_0 = 1.1$. However, for misalignment greater than about 2°, bending–torsion and bending–bending parametric instability zones begin to arise near $f_0 = (f_\phi + f_1)/2$ and $f_0 = f_1$, respectively.

For cases with non-zero external damping, $c_d > 0$, small amounts of misalignment continue to provide additional stabilization of the whirl boundary beyond the amount provided by the external damping (Figs. 4b, d, e and f). Note, this phenomena would also be seen in Fig. 4c but in this plot c_d is such that $f_w = 1.75$, hence the whirl boundary is outside the plot range for this graph. As the internal damping-induced whirl instability boundary is shifted to higher shaft speeds with increasing c_d, more misalignment induced sum-type bending–bending and torsion–bending parametric instability zones are revealed.

Bending–bending instability zones:

$$f_0 = f_1 + \rho, \quad f_0 = \tfrac{1}{4}(f_1 + f_2) + \rho \quad \text{and} \quad f_0 = \tfrac{1}{2}(f_1 + f_2) + \rho \quad \text{and} \quad f_0 = f_2 + \rho. \tag{29a}$$

Torsion–bending instability zones:

$$f_0 = \tfrac{1}{2}(f_\phi + f_1) + \rho \quad \text{and} \quad f_0 = \tfrac{1}{2}(f_\phi + f_2) + \rho. \tag{29b}$$

As seen in Eq. (29), the bending–bending combination frequencies are always supercritical, however the torsion–bending combination frequencies can be sub or supercritical depending on the torsional natural frequency f_ϕ. In this case, since $f_\phi = 0.125$, the first torque-bending instability is sub-critical, i.e., $f_0 = (f_\phi + f_1)/2 = 0.5625$ and the second torque-bending instability is supercritical, i.e., $f_0 = (f_\phi + f_2)/2 = 2.0625$. Finally, it is also apparent from Fig. 4, that the parametric instability regions occurring at higher shaft speeds have a wider frequency width for a given misalignment.

Fig. 5 shows the effect of non-zero load-torque, τ, on the misalignment-shaft speed instability regions. Here it is seen that, similar to misalignment, load-torque has both stabilizing and destabilizing effects. On one hand, load-torque is stabilizing since it tends to enhance the misalignment-induced stabilization of the whirl instability. This can be seen by comparing Fig. 4 with Fig. 5. This stabilization is most likely related to the asymmetric stiffness coupling matrix, $\mathbf{K}_0$, which is a function of misalignment, load-inertia, load-torque and shaft speed. This is consistent with the results from Zorzi and Nelson [1], where it was shown that bearing stiffness anisotropy delayed the whirl instability to higher speeds. In this case it is not bearing stiffness anisotropy, rather it is an effective stiffness anisotropy created by misalignment and load-torque acting through $\mathbf{K}_0$.

On the other hand, load-torque is destabilizing since it increases the size of the misalignment induced torsion–bending instability. Furthermore load-torque causes instability at the bending–bending instability zones independent of the misalignment. This is illustrated in Fig. 5 where the bending–bending instability zones have a finite frequency width even at zero misalignment.

4.3. Bending–bending parametric instability

In this sub-section, since misalignment and load-torque independently cause instability at shaft speeds near the sum-type bending–bending combination frequencies, both kinds of instability are examined. Figs. 6 and 7 show the effect of external damping on the load-torque and misalignment induced bending–bending instability regions.

Fig. 6 shows the misalignment induced bending–bending instability regions with $\tau = 0$ for several values of c_d. The size of the misalignment instability regions near $f_0 = f_1$ and $f_0 = (f_1 + f_2)/4$ are reduced by increasing the damping coefficient c_d (Fig. 6a). However, damping is not purely stabilizing for the instability region near $f_0 = (f_1 + f_2)/2$. In this case, damping increases the minimum value of destabilizing misalignment, but also increases the frequency width of the unstable region (Fig. 6b).

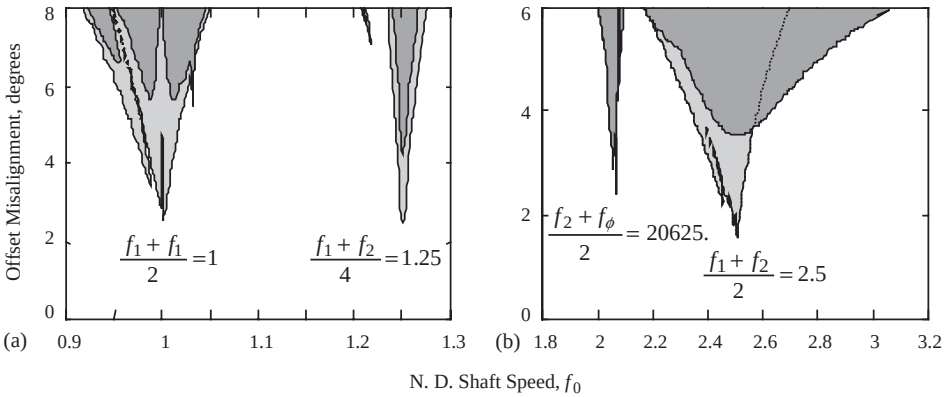

Fig. 6. Effect of damping on misalignment-induced bending–bending instability, $\tau = 0.0$. (a) □, $c_d = 0.002$; ■, $c_d = 0.02$ and (b) □, $c_d = 0.01$; ■, $c_d = 0.5$.

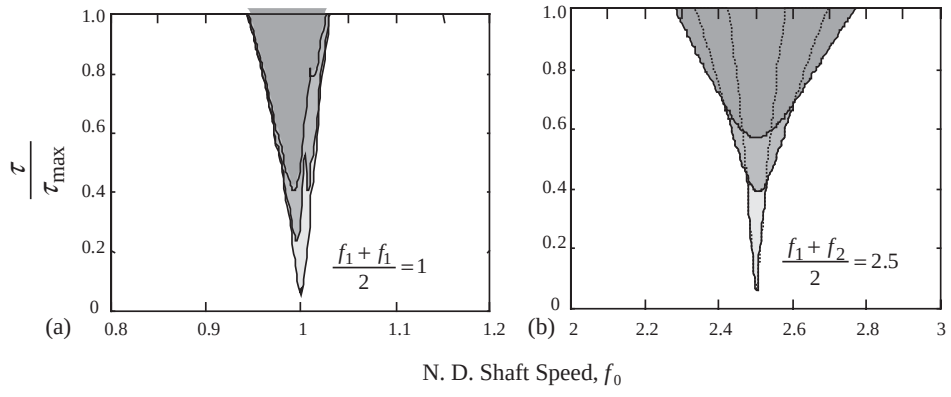

Fig. 7. Effect of damping on torque induced bending–bending instability, $\delta = \gamma = 0^\circ$. (a) □, $c_d = 0.002$; ■, $c_d = 0.01$; ■, $c_d = 0.02$ and (b) □, $c_d = 0.01$; ■, $c_d = 0.2$; ■, $c_d = 0.5$.

Fig. 7 shows the load-torque induced bending–bending instability regions with $\delta = \gamma = 0^\circ$ for several values of c_d. Here, again external damping tends to shrink the instability region near $f_0 = f_1$ but causes spreading of the instability region near $f_0 = (f_1 + f_2)/2$.

4.4. Torsion–bending parametric instability

In this sub-section, the behavior of the misalignment induced torsion–bending instability zones is studied. Fig. 8 and 9 show the first and second torque–bending instability zones near $f_0 = (f_\phi + f_1)/2$ and $f_0 = (f_\phi + f_2)/2$ for several values of external damping, c_d, and load-torque, τ. As seen from the plots and as noted in Section 4.2, the frequency width of both torsion–bending instability zones increases with load-torque. However, load-torque alone, without misalignment, is not sufficient to cause torsion–bending instability. Also, Fig. 8 shows that external damping, c_d, causes spreading of the first torsion–bending instability region.

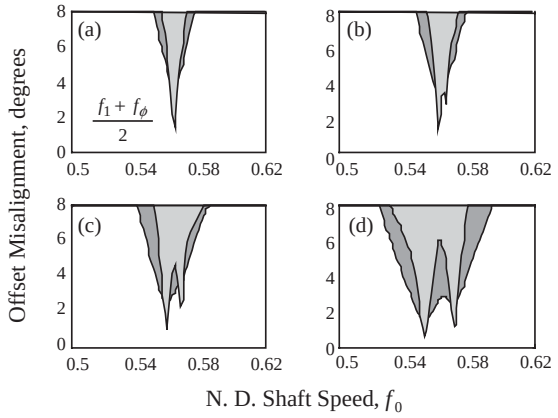

Fig. 8. Effect of damping, torque and misalignment on first torsion–bending instability. □, $c_d = 0.0$; ■, $c_d = 0.04$: (a) $\tau = 0.0$, (b) $\tau = 0.25\tau_{max}$, (c) $\tau = 0.5\tau_{max}$ and (d) $\tau = \tau_{max}$.

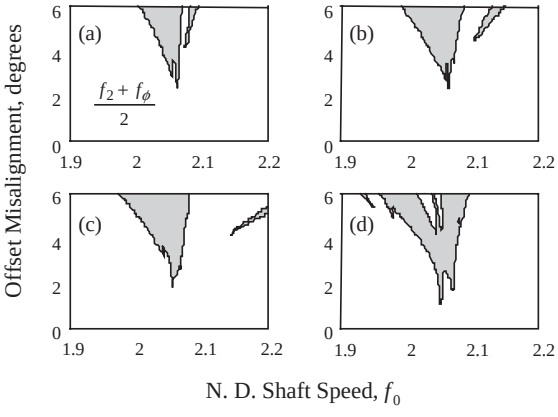

Fig. 9. Effect of damping, torque and misalignment on second torsion–bending instability. □, $c_d = 0.01$; ■, $c_d = 0.2$: (a) $\tau = 0.0$, (b) $\tau = 0.25\tau_{max}$, (c) $\tau = 0.5\tau_{max}$ and (d) $\tau = \tau_{max}$.

Finally, since the external damper does not supply damping to either the torsion mode or the second bending mode, increasing c_d has no effect on the 2nd torsion–bending instability, see Fig. 9.

5. Summary and conclusions

This research explores the effects of internal damping, external damping, misalignment, load-inertia and load-torque on the stability of a segmented shaft connected with U-Joint couplings operating at sub and supercritical speeds. A non-dimensional model is developed which includes both shaft bending and torsion flexibility along with the kinematic effects of static and dynamic misalignment as well as phasing and torque-windup between the U-Joints. In the equation-of-motion, internal damping results in both a damping matrix and a skew symmetric stiffness matrix, while the misalignment, load-inertia and load-torque result in constant and periodic inertia, damping, and stiffness coupling matrices, as well as forcing terms.

In the case with zero misalignment and zero load-torque, classic whirl instability occurs for shaft speeds above some supercritical operating speed that depends on the ratio of internal to external damping. When misalignment and load-torque are present, it is discovered that they both have stabilizing and destabilizing effects. For a given level of external damping, c_d, small amounts of misalignment, δ and γ, and load-torque, τ, tend to delay the onset of whirl instability beyond the nominal whirl-speed f_w. This whirl stabilization is most likely a consequence of the stiffness anisotropy created by the $\mathbf{K}_0$ coupling matrix.

Despite the whirl stabilization, misalignment and load-torque can create shaft speed zones of parametric instability in the sum-type combination frequency regions. Specifically, load-torque causes instability in the bending–bending regions while misalignment causes instability in both the bending–bending and torsion–bending regions. Furthermore, load-torque tends to increases the frequency width of the torsion–bending instability for a given level of misalignment.

The stability results for single U-Joint systems predict both torque induced bending–bending instability and misalignment induced torsion–bending instability, however misalignment induced bending–bending instability has not been identified in previous research. This phenomena can be explained by the presence of misalignment terms in the coupling matrices that allow periodic cross-coupling between bending modes giving rise to instability in these modes.

Finally, in addition to stabilizing whirl instability, the effectiveness of using external dampers to stabilize the parametric instability is investigated. It is shown that increasing the external damping, c_d, causes some parametric instability regions to shrink and others to spread. However, in both cases, increasing c_d is beneficial since it increases the minimum values of destabilizing torque and misalignment in the parametric instability zones.

Acknowledgements

This research is sponsored by the US Army Research Office MURI program with technical monitor Dr. Gary Anderson and by the NASA Graduate Student Research Program with NASA Glenn Research Center with technical monitor Andrew Provenza.

Appendix A. Non-dimensional system matrices

Nominal system matrices:

$$\bar{\mathbf{M}} = \begin{bmatrix} 1 & 0 & 0 & 0 & 0 & 0 & 0 & 0 & 0 \\ 0 & 1 & 0 & 0 & 0 & 0 & 0 & 0 & 0 \\ 0 & 0 & 1 & 0 & 0 & 0 & 0 & 0 & 0 \\ 0 & 0 & 0 & 1 & 0 & 0 & 0 & 0 & 0 \\ 0 & 0 & 0 & 0 & 1 & 0 & 0 & 0 & 0 \\ 0 & 0 & 0 & 0 & 0 & 1 & 0 & 0 & 0 \\ 0 & 0 & 0 & 0 & 0 & 0 & 1 & 0 & 0 \\ 0 & 0 & 0 & 0 & 0 & 0 & 0 & 1 & 0 \\ 0 & 0 & 0 & 0 & 0 & 0 & 0 & 0 & 1 \end{bmatrix},$$

$$\bar{\mathbf{G}} = f_0 \frac{\varepsilon^2 \pi^2}{8} \begin{bmatrix} 0 & f_1 & 0 & 0 & 0 & 0 & 0 & 0 & 0 \\ -f_1 & 0 & 0 & 0 & 0 & 0 & 0 & 0 & 0 \\ 0 & 0 & 0 & f_1 & 0 & 0 & 0 & 0 & 0 \\ 0 & 0 & -f_1 & 0 & 0 & 0 & 0 & 0 & 0 \\ 0 & 0 & 0 & 0 & 0 & f_2 & 0 & 0 & 0 \\ 0 & 0 & 0 & 0 & -f_2 & 0 & 0 & 0 & 0 \\ 0 & 0 & 0 & 0 & 0 & 0 & 0 & f_2 & 0 \\ 0 & 0 & 0 & 0 & 0 & 0 & -f_2 & 0 & 0 \\ 0 & 0 & 0 & 0 & 0 & 0 & 0 & 0 & 0 \end{bmatrix},$$

$$\bar{\mathbf{C}}_{sd} = \bar{\xi}_v \begin{bmatrix} f_1^2 & 0 & 0 & 0 & 0 & 0 & 0 & 0 & 0 \\ 0 & f_1^2 & 0 & 0 & 0 & 0 & 0 & 0 & 0 \\ 0 & 0 & f_1^2 & 0 & 0 & 0 & 0 & 0 & 0 \\ 0 & 0 & 0 & f_1^2 & 0 & 0 & 0 & 0 & 0 \\ 0 & 0 & 0 & 0 & f_2^2 & 0 & 0 & 0 & 0 \\ 0 & 0 & 0 & 0 & 0 & f_2^2 & 0 & 0 & 0 \\ 0 & 0 & 0 & 0 & 0 & 0 & f_2^2 & 0 & 0 \\ 0 & 0 & 0 & 0 & 0 & 0 & 0 & f_2^2 & 0 \\ 0 & 0 & 0 & 0 & 0 & 0 & 0 & 0 & f_\phi^2 \end{bmatrix},$$

$$\bar{\mathbf{C}}_{aux} = \begin{bmatrix} c_d & 0 & 0 & 0 & 0 & 0 & 0 & 0 & 0 \\ 0 & c_d & 0 & 0 & 0 & 0 & 0 & 0 & 0 \\ 0 & 0 & c_d & 0 & 0 & 0 & 0 & 0 & 0 \\ 0 & 0 & 0 & c_d & 0 & 0 & 0 & 0 & 0 \\ 0 & 0 & 0 & 0 & 0 & 0 & 0 & 0 & 0 \\ 0 & 0 & 0 & 0 & 0 & 0 & 0 & 0 & 0 \\ 0 & 0 & 0 & 0 & 0 & 0 & 0 & 0 & 0 \\ 0 & 0 & 0 & 0 & 0 & 0 & 0 & 0 & 0 \\ 0 & 0 & 0 & 0 & 0 & 0 & 0 & 0 & 0 \end{bmatrix},$$

$$\bar{\mathbf{K}} = \begin{bmatrix} f_1^2 & 0 & 0 & 0 & 0 & 0 & 0 & 0 & 0 \\ 0 & f_1^2 & 0 & 0 & 0 & 0 & 0 & 0 & 0 \\ 0 & 0 & f_1^2 & 0 & 0 & 0 & 0 & 0 & 0 \\ 0 & 0 & 0 & f_1^2 & 0 & 0 & 0 & 0 & 0 \\ 0 & 0 & 0 & 0 & f_2^2 & 0 & 0 & 0 & 0 \\ 0 & 0 & 0 & 0 & 0 & f_2^2 & 0 & 0 & 0 \\ 0 & 0 & 0 & 0 & 0 & 0 & f_2^2 & 0 & 0 \\ 0 & 0 & 0 & 0 & 0 & 0 & 0 & f_2^2 & 0 \\ 0 & 0 & 0 & 0 & 0 & 0 & 0 & 0 & f_\phi^2 \end{bmatrix},$$

$$\bar{\mathbf{K}}_{rd} = \bar{\xi}_v f_0 \begin{bmatrix} 0 & f_1^2 & 0 & 0 & 0 & 0 & 0 & 0 & 0 \\ -f_1^2 & 0 & 0 & 0 & 0 & 0 & 0 & 0 & 0 \\ 0 & 0 & 0 & f_1^2 & 0 & 0 & 0 & 0 & 0 \\ 0 & 0 & -f_1^2 & 0 & 0 & 0 & 0 & 0 & 0 \\ 0 & 0 & 0 & 0 & 0 & f_2^2 & 0 & 0 & 0 \\ 0 & 0 & 0 & 0 & -f_2^2 & 0 & 0 & 0 & 0 \\ 0 & 0 & 0 & 0 & 0 & 0 & 0 & f_2^2 & 0 \\ 0 & 0 & 0 & 0 & 0 & 0 & -f_2^2 & 0 & 0 \\ 0 & 0 & 0 & 0 & 0 & 0 & 0 & 0 & 0 \end{bmatrix}.$$

Inertia coupling matrices:

$$\bar{\mathbf{M}}_0 = \mu\pi^2 \begin{bmatrix} \frac{3\delta^2}{4} & 0 & -\frac{\delta\gamma}{4} & 0 & \frac{3\delta^2}{2} & 0 & \frac{\delta\gamma}{2} & 0 & \frac{\delta}{2\pi} \\ 0 & \frac{\delta^2}{4} & 0 & \frac{\delta\gamma}{4} & 0 & \frac{\delta^2}{2} & 0 & -\frac{\delta\gamma}{2} & 0 \\ -\frac{\delta\gamma}{4} & 0 & \frac{3\gamma^2}{4} & 0 & -\frac{\delta\gamma}{2} & 0 & -\frac{3\gamma^2}{2} & 0 & -\frac{\gamma}{2\pi} \\ 0 & \frac{\delta\gamma}{4} & 0 & \frac{\gamma^2}{4} & 0 & \frac{\delta\gamma}{2} & 0 & -\frac{\gamma^2}{2} & 0 \\ \frac{3\delta^2}{2} & 0 & -\frac{\delta\gamma}{2} & 0 & 3\delta^2 & 0 & \delta\gamma & 0 & \frac{\delta}{\pi} \\ 0 & \frac{\delta^2}{2} & 0 & \frac{\delta\gamma}{2} & 0 & \delta^2 & 0 & -\delta\gamma & 0 \\ \frac{\delta\gamma}{2} & 0 & -\frac{3\gamma^2}{2} & 0 & \delta\gamma & 0 & 3\gamma^2 & 0 & \frac{\gamma}{\pi} \\ 0 & -\frac{\delta\gamma}{2} & 0 & -\frac{\gamma^2}{2} & 0 & -\delta\gamma & 0 & \gamma^2 & 0 \\ \frac{\delta}{\mu\pi} & 0 & -\frac{\gamma}{\mu\pi} & 0 & \frac{2\delta}{\mu\pi} & 0 & \frac{2\gamma}{\mu\pi} & 0 & 0 \end{bmatrix},$$

$$\bar{\mathbf{M}}_{s2} = \mu\pi^2 \begin{bmatrix} 0 & -\frac{\delta^2}{2} & 0 & -\frac{\delta\gamma}{2} & 0 & -\delta^2 & 0 & \delta\gamma & 0 \\ -\frac{\delta^2}{2} & 0 & \frac{\delta\gamma}{2} & 0 & -\delta^2 & 0 & -\delta\gamma & 0 & -\frac{\delta}{2\pi} \\ 0 & \frac{\delta\gamma}{2} & 0 & \frac{\gamma^2}{2} & 0 & \delta\gamma & 0 & -\gamma^2 & \frac{\gamma\phi_s}{\pi} \\ -\frac{\delta\gamma}{2} & 0 & \frac{\gamma^2}{2} & 0 & -\delta\gamma & 0 & -\gamma^2 & 0 & -\frac{\gamma}{2\pi} \\ 0 & -\delta^2 & 0 & -\delta\gamma & 0 & -2\delta^2 & 0 & 2\delta\gamma & 0 \\ -\delta^2 & 0 & \delta\gamma & 0 & -2\delta^2 & 0 & -2\delta\gamma & 0 & -\frac{\delta}{\pi} \\ 0 & -\delta\gamma & 0 & -\gamma^2 & 0 & -2\delta\gamma & 0 & 2\gamma^2 & -\frac{2\gamma\phi_s}{\pi} \\ \delta\gamma & 0 & -\gamma^2 & 0 & 2\delta\gamma & 0 & 2\gamma^2 & 0 & \frac{\gamma}{\pi} \\ 0 & -\frac{\delta}{\mu\pi} & \frac{2\gamma\phi_s}{\mu\pi} & -\frac{\gamma}{\mu\pi} & 0 & -\frac{2\delta}{\mu\pi} & -\frac{4\gamma\phi_s}{\mu\pi} & \frac{2\gamma}{\mu\pi} & 0 \end{bmatrix},$$

$$\bar{\mathbf{M}}_{c2} = \mu\pi^2 \begin{bmatrix} -\delta^2 & 0 & 0 & 0 & -2\delta^2 & 0 & 0 & 0 & -\frac{\delta}{2\pi} \\ 0 & 0 & 0 & 0 & 0 & 0 & 0 & 0 & 0 \\ 0 & 0 & \gamma^2 & 0 & 0 & 0 & -2\gamma^2 & 0 & -\frac{\gamma}{2\pi} \\ 0 & 0 & 0 & 0 & 0 & 0 & 0 & 0 & -\frac{\gamma\phi_s}{\pi} \\ -2\delta^2 & 0 & 0 & 0 & -4\delta^2 & 0 & 0 & 0 & -\frac{\delta}{\pi} \\ 0 & 0 & 0 & 0 & 0 & 0 & 0 & 0 & 0 \\ 0 & 0 & -2\gamma^2 & 0 & 0 & 0 & 4\gamma^2 & 0 & \frac{\gamma}{\pi} \\ 0 & 0 & 0 & 0 & 0 & 0 & 0 & 0 & \frac{2\gamma\phi_s}{\pi} \\ -\frac{\delta}{\mu\pi} & 0 & -\frac{\gamma}{\mu\pi} & -\frac{2\gamma\phi_s}{\mu\pi} & -\frac{2\delta}{\mu\pi} & 0 & \frac{2\gamma}{\mu\pi} & \frac{4\gamma\phi_s}{\mu\pi} & -\frac{\gamma^2}{\mu\pi^2} \end{bmatrix}.$$

Damping coupling matrices:

$$\bar{\mathbf{C}}_0 = f_0\mu\pi^2\begin{bmatrix} 0 & \delta^2 & 0 & \delta\gamma & 0 & 2\delta^2 & 0 & -2\delta\gamma & 0 \\ -\delta^2 & 0 & -\delta\gamma & 0 & -2\delta^2 & 0 & 2\delta\gamma & 0 & 0 \\ 0 & \delta\gamma & 0 & \gamma^2 & 0 & 2\delta\gamma & 0 & -2\gamma^2 & 0 \\ -\delta\gamma & 0 & -\gamma^2 & 0 & -2\delta\gamma & 0 & 2\gamma^2 & 0 & 0 \\ 0 & 2\delta^2 & 0 & 2\delta\gamma & 0 & 4\delta^2 & 0 & -4\delta\gamma & 0 \\ -2\delta^2 & 0 & -2\delta\gamma & 0 & -4\delta^2 & 0 & 4\delta\gamma & 0 & 0 \\ 0 & -2\delta\gamma & 0 & -2\gamma^2 & 0 & -4\delta\gamma & 0 & 4\gamma^2 & 0 \\ 2\delta\gamma & 0 & 2\gamma^2 & 0 & 4\delta\gamma & 0 & -4\gamma^2 & 0 & 0 \\ 0 & 0 & 0 & 0 & 0 & 0 & 0 & 0 & 0 \end{bmatrix},$$

$$\bar{\mathbf{C}}_{s2} = f_0\mu\pi^2\begin{bmatrix} 2\delta^2 & 0 & 2\delta\gamma & 0 & 4\delta^2 & 0 & -4\delta\gamma & 0 & 0 \\ 0 & 0 & 0 & 0 & 0 & 0 & 0 & 0 & 0 \\ -2\delta\gamma & 0 & -2\gamma^2 & 0 & -4\delta\gamma & 0 & 4\gamma^2 & 0 & 0 \\ 0 & 0 & 0 & 0 & 0 & 0 & 0 & 0 & 0 \\ 4\delta^2 & 0 & 4\delta\gamma & 0 & 8\delta^2 & 0 & -8\delta\gamma & 0 & 0 \\ 0 & 0 & 0 & 0 & 0 & 0 & 0 & 0 & 0 \\ 4\delta\gamma & 0 & 4\gamma^2 & 0 & 8\delta\gamma & 0 & -8\gamma^2 & 0 & 0 \\ 0 & 0 & 0 & 0 & 0 & 0 & 0 & 0 & 0 \\ \frac{4\delta}{\mu\pi} & 0 & \frac{4\gamma}{\mu\pi} & \frac{8\gamma\phi_s}{\mu\pi} & \frac{8\delta}{\mu\pi} & 0 & -\frac{8\gamma}{\mu\pi} & -\frac{16\gamma\phi_s}{\mu\pi} & \frac{2\gamma^2}{\mu\pi^2} \end{bmatrix},$$

$$\bar{\mathbf{C}}_{c2} = f_0\mu\pi^2\begin{bmatrix} 0 & -2\delta^2 & 0 & -2\delta\gamma & 0 & -4\delta^2 & 0 & 4\delta\gamma & 0 \\ 0 & 0 & 0 & 0 & 0 & 0 & 0 & 0 & 0 \\ 0 & 2\delta\gamma & 0 & 2\gamma^2 & 0 & 4\delta\gamma & 0 & -4\gamma^2 & 0 \\ 0 & 0 & 0 & 0 & 0 & 0 & 0 & 0 & 0 \\ 0 & -4\delta^2 & 0 & -4\delta\gamma & 0 & -8\delta^2 & 0 & 8\delta\gamma & 0 \\ 0 & 0 & 0 & 0 & 0 & 0 & 0 & 0 & 0 \\ 0 & -4\delta\gamma & 0 & -4\gamma^2 & 0 & -8\delta\gamma & 0 & 8\gamma^2 & 0 \\ 0 & 0 & 0 & 0 & 0 & 0 & 0 & 0 & 0 \\ 0 & -\frac{4\delta}{\mu\pi} & \frac{8\gamma\phi_s}{\mu\pi} & -\frac{4\gamma}{\mu\pi} & 0 & -\frac{8\delta}{\mu\pi} & -\frac{16\gamma\phi_s}{\mu\pi} & \frac{8\gamma}{\mu\pi} & 0 \end{bmatrix}.$$

Stiffness coupling matrices:

$$\bar{K}_0 = f_0^2\mu\pi^2\begin{bmatrix} -\delta^2 & 0 & -\frac{1}{2}(\delta+\gamma)^2 & 0 & 2\gamma^2 & 0 & -(\delta-\gamma)^2 & 0 & 0 \\ 0 & -\delta^2 & 0 & \frac{1}{2}(\delta-\gamma)^2 & 0 & -4\delta^2-2\gamma^2 & 0 & (\delta+\gamma)^2 & 0 \\ -\frac{1}{2}(\delta+\gamma)^2 & 0 & -\gamma^2 & 0 & (\delta-\gamma)^2 & 0 & -2\delta^2 & 0 & 0 \\ 0 & \frac{1}{2}(\delta-\gamma)^2 & 0 & -\gamma^2 & 0 & -(\delta+\gamma)^2 & 0 & 2\delta^2+4\gamma^2 & 0 \\ 2\gamma^2 & 0 & (\delta-\gamma)^2 & 0 & -4\delta^2 & 0 & 2(\delta+\gamma)^2 & 0 & 0 \\ 0 & -4\delta^2-2\gamma^2 & 0 & -(\delta+\gamma)^2 & 0 & -4\delta^2 & 0 & -2(\delta-\gamma)^2 & 0 \\ -(\delta-\gamma)^2 & 0 & -2\delta^2 & 0 & 2(\delta+\gamma)^2 & 0 & -4\gamma^2 & 0 & 0 \\ 0 & (\delta+\gamma)^2 & 0 & 2\delta^2+4\gamma^2 & 0 & -2(\delta-\gamma)^2 & 0 & -4\gamma^2 & 0 \\ 0 & 0 & 0 & 0 & 0 & 0 & 0 & 0 & 0 \end{bmatrix}$$

$$+\tau\pi^2\begin{bmatrix} 0 & 0 & 0 & -1 & 0 & 0 & 0 & -2 & 0 \\ 0 & 0 & 1 & 0 & 0 & 0 & 2 & 0 & 0 \\ 0 & 1 & 0 & 0 & 0 & -2 & 0 & 0 & 0 \\ -1 & 0 & 0 & 0 & 2 & 0 & 0 & 0 & 0 \\ 0 & 0 & 0 & 2 & 0 & 0 & 0 & 4 & 0 \\ 0 & 0 & -2 & 0 & 0 & 0 & -4 & 0 & 0 \\ 0 & 2 & 0 & 0 & 0 & -4 & 0 & 0 & 0 \\ -2 & 0 & 0 & 0 & 4 & 0 & 0 & 0 & 0 \\ 0 & 0 & 0 & 0 & 0 & 0 & 0 & 0 & 0 \end{bmatrix},$$

$$\bar{\mathbf{K}}_{c2} = f_0^2\mu\pi^2\begin{bmatrix} 2\delta^2 & 0 & 2\delta\gamma & 0 & 4\delta^2 & 0 & -4\delta\gamma & 0 & 0 \\ 0 & 0 & 0 & 0 & 0 & 0 & 0 & 0 & 0 \\ -2\delta\gamma & 0 & -2\gamma^2 & 0 & -4\delta\gamma & 0 & 4\gamma^2 & 0 & 0 \\ 0 & 0 & 0 & 0 & 0 & 0 & 0 & 0 & 0 \\ 4\delta^2 & 0 & 4\delta\gamma & 0 & 8\delta^2 & 0 & -8\delta\gamma & 0 & 0 \\ 0 & 0 & 0 & 0 & 0 & 0 & 0 & 0 & 0 \\ 4\delta\gamma & 0 & 4\gamma^2 & 0 & 8\delta\gamma & 0 & -8\gamma^2 & 0 & 0 \\ 0 & 0 & 0 & 0 & 0 & 0 & 0 & 0 & 0 \\ \frac{4\delta}{\mu\pi} & 0 & \frac{4\gamma}{\mu\pi} & \frac{8\gamma\phi_s}{\mu\pi} & \frac{8\delta}{\mu\pi} & 0 & -\frac{8\gamma}{\mu\pi} & -\frac{16\gamma\phi_s}{\mu\pi} & \frac{2\gamma^2}{\mu\pi^2} \end{bmatrix}$$

$$+\tau\pi^2\begin{bmatrix} -\phi_s & 0 & -\phi_s & 1 & 2\phi_s & -4 & -2\phi_s & 2 & 0 \\ 0 & \phi_s & 1 & \phi_s & -4 & -2\phi_s & 2 & 2\phi_s & 0 \\ -\phi_s & 1 & \phi_s & 0 & 2\phi_s & -2 & -6\phi_s & 4 & 0 \\ 1 & \phi_s & 0 & -\phi_s & -2 & -2\phi_s & 4 & 6\phi_s & -\frac{\gamma}{\pi} \\ 2\phi_s & -4 & 2\phi_s & -2 & -4\phi_s & 0 & 4\phi_s & -4 & 0 \\ -4 & -2\phi_s & -2 & -2\phi_s & 0 & 4\phi_s & -4 & -4\phi_s & 0 \\ -2\phi_s & 2 & -6\phi_s & 4 & 4\phi_s & -4 & 4\phi_s & 0 & 0 \\ 2 & 2\phi_s & 4 & 6\phi_s & -4 & -4\phi_s & 0 & -4\phi_s & \frac{2\gamma}{\pi} \\ 0 & 0 & 0 & -\frac{2\gamma}{\mu\pi} & 0 & 0 & 0 & \frac{4\gamma}{\mu\pi} & 0 \end{bmatrix},$$

$$\bar{K}_{s2} = f_0^2\mu\pi^2\begin{bmatrix} 0 & 2\delta^2 & 0 & -(\delta-\gamma)^2 & 0 & 4\delta^2 & 0 & -2(\delta+\gamma)^2 & 0 \\ 0 & 0 & \delta^2+\gamma^2 & 0 & 0 & 0 & 2(\delta^2+\gamma^2) & 0 & 0 \\ 0 & (\delta-\gamma)^2 & 0 & -2\gamma^2 & 0 & -2(\delta+\gamma)^2 & 0 & 4\gamma^2 & 0 \\ -(\delta^2+\gamma^2) & 0 & 0 & 0 & 2(\delta^2+\gamma^2) & 0 & 0 & 0 & 0 \\ 0 & 4\delta^2 & 0 & 2(\delta+\gamma)^2 & 0 & 8\delta^2 & 0 & 4(\delta-\gamma)^2 & 0 \\ 0 & 0 & -2(\delta^2+\gamma^2) & 0 & 0 & 0 & -4(\delta^2+\gamma^2) & 0 & 0 \\ 0 & 2(\delta+\gamma)^2 & 0 & 4\gamma^2 & 0 & -4(\delta-\gamma)^2 & 0 & -8\gamma^2 & 0 \\ -2(\delta^2+\gamma^2) & 0 & 0 & 0 & 4(\delta^2+\gamma^2) & 0 & 0 & 0 & 0 \\ 0 & \frac{4\delta}{\mu\pi} & -\frac{8\gamma\phi_s}{\mu\pi} & \frac{4\gamma}{\mu\pi} & 0 & \frac{8\delta}{\mu\pi} & \frac{16\gamma\phi_s}{\mu\pi} & -\frac{8\gamma}{\mu\pi} & 0 \end{bmatrix}$$

$$+\tau\pi^2\begin{bmatrix} 0 & -\phi_s & -1 & -\phi_s & 4 & 2\phi_s & -2 & -2\phi_s & 0 \\ -\phi_s & 0 & -\phi_s & 1 & 2\phi_s & -4 & -2\phi_s & 2 & 0 \\ -1 & -\phi_s & 0 & \phi_s & 2 & 2\phi_s & -4 & -6\phi_s & \frac{\gamma}{\pi} \\ -\phi_s & 1 & \phi_s & 0 & 2\phi_s & -2 & -6\phi_s & 4 & 0 \\ 4 & 2\phi_s & 2 & 2\phi_s & 0 & -4\phi_s & 4 & 4\phi_s & 0 \\ 2\phi_s & -4 & 2\phi_s & -2 & -4\phi_s & 0 & 4\phi_s & -4 & 0 \\ -2 & -2\phi_s & -4 & -6\phi_s & 4 & 4\phi_s & 0 & 4\phi_s & -\frac{2\gamma}{\pi} \\ -2\phi_s & 2 & -6\phi_s & 4 & 4\phi_s & -4 & 4\phi_s & 0 & 0 \\ 0 & 0 & \frac{2\gamma}{\mu\pi} & 0 & 0 & 0 & -\frac{4\gamma}{\mu\pi} & 0 & 0 \end{bmatrix}.$$

Forcing terms:

$$\mathbf{F}_0 = f_0^2\mu\pi\begin{bmatrix} 0 \\ \frac{\delta^3}{4}+\frac{\delta\gamma^2}{4} \\ 0 \\ \frac{\delta^2\gamma}{4}+\frac{\gamma^3}{4} \\ 0 \\ \frac{\delta^3}{2}+\frac{\delta\gamma^2}{2} \\ 0 \\ -\frac{\delta^2\gamma}{2}-\frac{\gamma^3}{2} \\ 0 \end{bmatrix} + \tau\pi\begin{bmatrix} -\frac{\delta}{2}+\frac{\gamma}{2} \\ 0 \\ -\frac{\delta}{2}-\frac{\gamma}{2} \\ 0 \\ -\delta-\gamma \\ 0 \\ \delta-\gamma \\ 0 \\ 0 \end{bmatrix},$$

$$\mathbf{F}_{s2} = f_0^2\mu\pi\begin{bmatrix} -\frac{\delta^3}{2}-\frac{\delta\gamma^2}{2} \\ 0 \\ \frac{\delta^2\gamma}{2}+\frac{\gamma^3}{2} \\ 0 \\ -\delta^3-\delta\gamma^2 \\ 0 \\ -\delta^2\gamma-\gamma^3 \\ 0 \\ -\frac{\delta^2}{\mu\pi}-\frac{\gamma^2}{\mu\pi} \end{bmatrix} + \tau\pi\begin{bmatrix} -\gamma\phi_s \\ \frac{\delta}{2}+\frac{\gamma}{2}-\gamma\phi_s^2 \\ \gamma\phi_s \\ \frac{\delta}{2}-\frac{\gamma}{2}+\gamma\phi_s^2 \\ 2\gamma\phi_s \\ \delta-\gamma+2\gamma\phi_s^2 \\ 2\gamma\phi_s \\ -\delta-\gamma+2\gamma\phi_s^2 \\ -\frac{\gamma^2\phi_s}{\mu\pi} \end{bmatrix},$$

$$\mathbf{F}_{c2} = f_0^2\mu\pi\begin{bmatrix} 0 \\ 0 \\ 0 \\ 0 \\ 0 \\ 0 \\ 0 \\ 0 \\ -\frac{2\gamma^2\phi_s}{\mu\pi} \end{bmatrix} + \tau\pi\begin{bmatrix} \frac{\delta}{2}+\frac{\gamma}{2}-\gamma\phi_s^2 \\ \gamma\phi_s \\ \frac{\delta}{2}-\frac{\gamma}{2}+\gamma\phi_s^2 \\ -\gamma\phi_s \\ \delta-\gamma+2\gamma\phi_s^2 \\ -2\gamma\phi_s \\ -\delta-\gamma+2\gamma\phi_s^2 \\ -2\gamma\phi_s \\ \frac{\gamma^2}{2\mu\pi} \end{bmatrix}.$$

References

[1] E.S. Zorzi, H.D. Nelson, Finite element simulation of rotor-bearing systems with internal damping, *American Society for Mechanical Engineers, Journal of Engineering for Power* 99 (1977) 71–76.
[2] L.W. Chen, D.M. Ku, Finite element analysis of natural whirl speeds of rotating shafts, *Computers and Structures* 40 (1991) 741–747.
[3] T. Iwatsubo, M. Saigo, Transverse vibration of a rotor system driven by a Cardan joint, *Journal of Sound and Vibration* 95 (1984) 9–18.
[4] A.J. Mazzei Jr., A. Argento, R.A. Scott, Dynamic stability of a rotating shaft driven through a universal joint, *Journal of Sound and Vibration* 222 (1999) 19–47.
[5] S.F. Asokanthan, M.C. Hwang, Torsional instabilities in a system incorporating a Hooke's joint, *Journal of Vibration and Acoustics* 118 (1996) 368–374.
[6] S.F. Asokanthan, X.H. Wang, Characterization of torsional instabilities in a Hooke's joint driven system via maximal Lyapunov exponents, *Journal of Sound and Vibration* 194 (1996) 83–91.
[7] H.A. DeSmidt, K.W. Wang, E.C. Smith, Coupled torsion–lateral stability of a shaft–disk system driven through a universal joint, *American Society for Mechanical Engineers, Journal of Applied Mechanics* 69 (2002) 261–273.
[8] M. Kato, H. Ota, Lateral excitation of a rotating shaft driven by a universal joint with friction, *Journal of Vibration and Acoustics* 112 (1990) 298–303.
[9] M. Xu, R.D. Marangoni, Vibration analysis of a motor-flexible coupling-rotor system subjected to misalignment and unbalance. Part I: theoretical model and analysis, *Journal of Sound and Vibration* 176 (1994) 663–679.
[10] R.M. Rosenberg, T. Ohio, On the dynamical behavior of rotating shafts driven by universal (Hooke) coupling, *American Society for Mechanical Engineers, Journal of Applied Mechanics* 25 (1958) 47–51.
[11] P.P. Sheu, W.H. Chieng, A.C. Lee, Modeling and analysis of the intermediate shaft between two universal joints, *Journal of Vibration and Acoustics* 118 (1996) 88–99.
[12] V.V. Bolotin, *Nonconservative Problems of the Theory of Elastic Stability*, Pergamon Press, New York, 1963.
[13] C.S. Hsu, On the parametric excitation of a dynamic system having multiple degrees of freedom, *American Society for Mechanical Engineers, Journal of Applied Mechanics* 30 (1963) 367–372.